Design of a Novel Loosely Coupled Parallel Structural Upper Body Exoskeleton

Xinhui Tian, Xin Zhou, Bin Xie*

***Abstract*— Exoskeletons, as wearable human–robot collaborative devices, can effectively reduce muscle fatigue caused by prolonged material handling and overhead tasks. However, most existing active exoskeletons adopt tightly coupled serial structures, which generally suffer from insufficient wearing comfort, limited muscle coverage, and restricted workspace. To address these issues, this paper presents a novel loosely coupled, parallel upper-body exoskeleton (6.9 kg). The proposed exoskeleton is connected only at the waist and elbow, providing assistance not only to the small muscle groups of the arms and shoulders but also to the larger muscle groups of the waist, back, and chest. Moreover, heavy components of the exoskeleton (approximately 78% of the total mass), such as actuators are located near the wearer's waist, which places the center of mass close to the human center of mass, improving comfort and control reliability. To validate the feasibility of the design, kinematic models of both the exoskeleton and the human upper body were established. Analysis showed that the end-effector workspace of the exoskeleton exceeds that of the human elbow. Prototype experiments were conducted, allowing the wearer to perform arbitrary postures without constraining spinal motion. This indicates that the exoskeleton holds potential in work assistance scenarios such as long-term heavy lifting and overhead work.**

I. Introduction

In daily operations in industries such as manufacturing, warehousing and logistics, and construction, workers are often required to perform long-duration tasks such as heavy material handling and overhead installation. These tasks typically demand continuous activation of the upper-body muscle groups, especially the muscles of the lower back, back, shoulders, and arms. When these muscles remain under high load for extended periods, muscle fatigue is likely to occur. Muscle fatigue not only reduces operational efficiency but may also increase the risk of occupational injuries such as muscle strain and spinal damage, posing a serious threat to workers' health and safety [1], [2]. Therefore, the development of assistive equipment capable of effectively alleviating upper-body muscle load and supporting workers in completing high-intensity tasks has become an important research direction in the fields of occupational health and engineering equipment.

Exoskeletons, as a type of wearable human-robot collaborative equipment, can effectively reduce the muscular burden of the human body by coordinating with human movements and providing assistive forces. They have become one of the key technologies for addressing the problems. Among them, active exoskeletons, due to their ability to actively output assistive force, show great potential in operation assistance and have attracted extensive attention from both academia and industry. However, most existing active exoskeletons adopt tightly coupled and serial structures. Although these designs can achieve certain assistive functions, they have obvious limitations [3], [4], [5], [6].

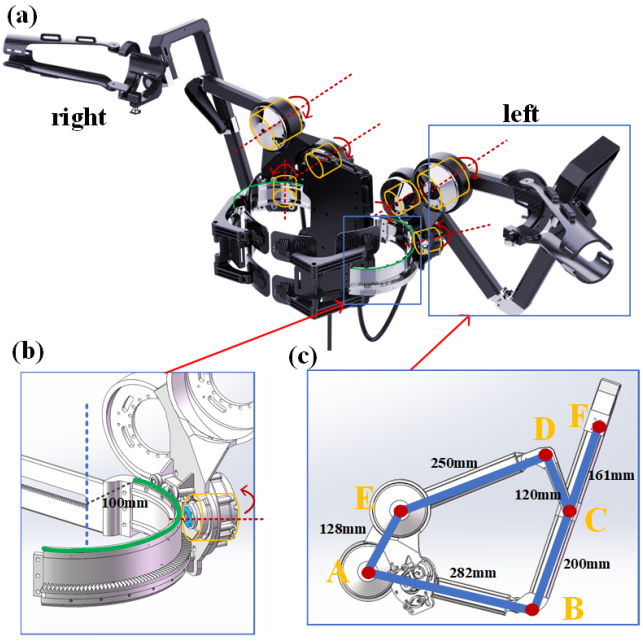

Fig. 1. Novel loosely-coupled parallel structural upper-body exoskeleton: (a) overall structure, (b) circular waist-rail mechanism ($R = 100$ mm), and (c) planar five-bar parallel mechanism with link lengths $L_{AB} = 282$ mm, $L_{BC} = 200$ mm, $L_{CD} = 120$ mm, $L_{DE} = 250$ mm, $L_{AE} = 128$ mm, and $L_{CF} = 161$ mm.

The tightly coupled connections often require the exoskeleton to closely fit multiple parts of the human body, which easily constrains natural human movement and results in poor wearing comfort. Meanwhile, the assistive range of serial structures is relatively limited, mostly focusing on specific joints or local muscle groups. This makes it difficult to cover the large range of upper-body muscle activation needs, and the workspace is also restricted by the structure itself, making it less adaptable to complex and variable working postures. These issues greatly restrict the practical effectiveness of active exoskeletons in long-term and complex operation scenarios [7], [8], [9], [10], [11], [12].

In contrast, parallel structures have significant advantages in terms of the magnitude and range of assistance, which

Xinhui Tian, Xin Zhou and Bin Xie are with School of Automation, Central South University, Changsha, China.Xinhui Tian and Xin Zhou contributed equally to this work and share co-first authorship. Bin Xie is the corresponding author (email: xiebin@csu.edu.cn).

gives them broad application prospects in exoskeleton design [13], [14], [15], [16]. Therefore, developing an upper-body exoskeleton that balances comfort, muscle coverage, and motion flexibility is of great practical significance to address the problems of insufficient comfort, limited muscle coverage, and restricted workspace in existing active exoskeletons. In this paper, a novel loosely coupled parallel structure upper-body exoskeleton is designed to effectively solve the above problems. The main contributions of this article are as follows:

- A novel loosely coupled parallel structure upper-body exoskeleton (6.9 kg) is proposed, as shown in Fig. 1. The exoskeleton is connected only at the waist and elbow, providing assistance not only to the small muscle groups of the arms and shoulders but also to the larger muscle groups of the waist, back, and chest.
- A parallel structure is adopted, heavy components of the exoskeleton (approximately 78% of the total mass), such as actuators are located near the wearer's waist, while the relatively high-speed moving links are made of carbon fiber. This design places the overall center of mass closer to the human center of mass and reduces the effect of inertia on control performance.
- Kinematic models of both the exoskeleton and the human upper body are established, and analysis shows that the end-effector workspace of the exoskeleton exceeds that of the human elbow. Prototype experiments demonstrate that the wearer can perform a wide range of extreme postures without any constraint on natural motion.

II. STRUCTURE DESIGN

A. Analysis of Upper-Body Degrees of Freedom

To achieve wearer comfort, it is necessary to first analyze the DOF of the human upper body.As shown in Fig. 2(a), the human back, i.e., the spinal column (including the lumbar and thoracic vertebrae), exhibits three types of motions resulting from spinal DOF: flexion and extension, lateral flexion, and rotation. In serial structure upper-limb exoskeleton design, the high redundancy of spinal DOF is often ignored. However, neglecting these DOF can cause stiffness in the upper body of the wearer. During overhead tasks, this stiffness may lead to imbalance of the body's center of gravity and even cause falls, posing safety risks. On the other hand, in daily life or light work scenarios, ignoring the spinal DOF can help protect the lumbar spine during flexion and extension motions, keeping the lumbar region relatively stable and reducing wear — which is why most lumbar-assist exoskeletons are designed this way. Nevertheless, in lateral bending and rotational motions, such exoskeletons impose constraints, forcing the user to translate or rotate the entire torso to reach the desired workspace. Therefore, to avoid reducing human flexibility, the spinal DOF should not be disregarded. Fig. 2(b) illustrates the mobility of the sternoclavicular joint, where the clavicle performs three types of motions: protraction and retraction,elevation and depression. Fig. 2(c) shows that the glenohumeral joint three types of motions: elevation/depression, protraction/retraction, and internal/external rotation. Due to the high redundancy of the human upper-body DOF, some exoskeleton designs omit the shoulder girdle structure to reduce weight. However, this omission may result in acromion impingement, humeral head dislocation, and muscle injuries. A comparison with the upper-body DOF reveals that conventional serial-type exoskeletons generally only replicate the glenohumeral joint, while neglecting the spinal joints and sternoclavicular joints in their tightly coupled designs. Ferreira [17] reported that after four weeks of wearing a serial exoskeleton, workers showed a significant decrease in willingness to wear the device. This was attributed not only to joint and tissue pain caused by neglecting human anatomical structures but also to the stiffness and heaviness of the exoskeleton itself, which is particularly dangerous in overhead operations. Therefore, to maximize coverage of the upper-body DOF and improve wearer comfort, the novel loosely coupled parallel exoskeleton proposed in this work is designed to cover the vast majority of the upper-body DOF, thus avoiding joint pain and other issues caused by neglecting natural human mobility.

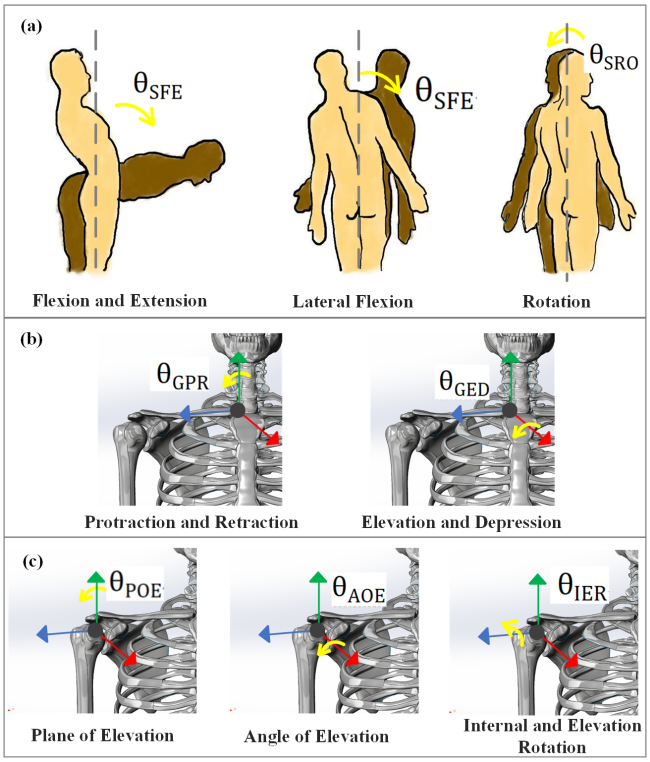

Fig. 2. Human upper-body DOF: (a) spinal DOF, (b) sternoclavicular joint DOF, and (c) glenohumeral joint DOF.

B. Analysis of the Loosely-Coupled Parallel Upper-Body Exoskeleton Structure

Considering the bilateral symmetry of the human body, the proposed upper-body exoskeleton is designed to be symmetric as well. Therefore, only the left half of the exoskeleton is analyzed here for clarity. As shown in Fig. 1,

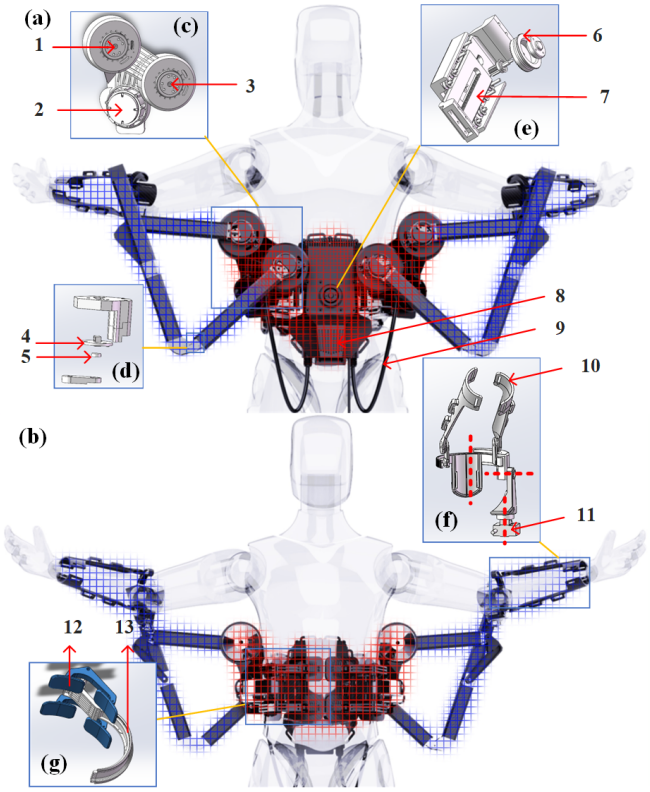

Fig. 3. Novel Loosely-Coupled Parallel Upper-Body Exoskeleton Structure View: (a) Rear view of the exoskeleton, (b) Front view of the exoskeleton, (c) Joint motors, (d) Passive joints, (e) Waist width adjustment device, (f) Elbow binding fixture, (g) Adaptive waist support. 1. DM4340P joint motor 1; 2. CyberGear joint motor; 3. DM4340P joint motor 2; 4. MT6835 magnetic encoder; 5. Magnet; 6. Waist ratchet disk; 7. Slider; 8. Power supply and PCB; 9. Cable harness; 10. Small waist binding strap; 11. 3D force sensor; 12. Adaptive waist plate; 13. Circular waist rail.

the active DOF of the exoskeleton can be divided into two parts. The first part, shown in Fig. 1(b), is a circular waist-rail mechanism that primarily controls the horizontal abduction and adduction of the arm, corresponding to the DOF on the horizontal plane. It consists of a circular sliding rail and Joint Motor 1, which is mounted with an extended bearing to counteract bending torques. A straight-toothed gear mechanism is adopted because it conforms to the contour of the human waist, satisfies the horizontal plane DOF requirements, and is capable of generating large thrust forces.The second part, as shown in Fig. 1(c), is a planar five-bar parallel mechanism, which is responsible for the degrees of freedom in the sagittal and coronal planes of the human body, namely arm elevation and lowering. Although this mechanism consists of five links, it effectively provides only two degrees of freedom. The mechanism is driven by Joint Motor 2 and Joint Motor 3 as the actuated joints. All links and connectors are made of aluminum alloy and carbon fiber rods to achieve lightweight design while maintaining sufficient stiffness. A three-dimensional force sensor is rigidly attached to the end-effector of the five-bar linkage to measure the interaction forces between the human elbow and the exoskeleton in three directions. This design allows the human elbow joint to translate within a

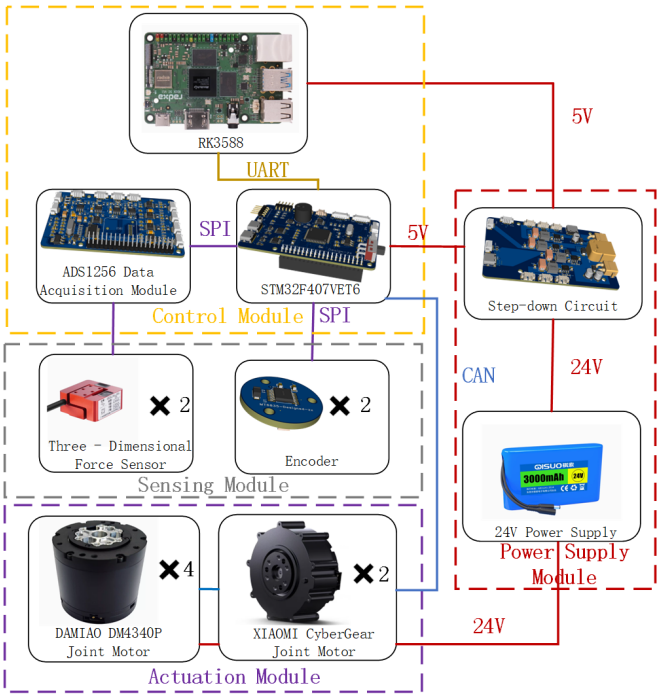

Fig. 4. Exoskeleton control system

Cartesian coordinate frame, while rotational motions of the arm are accommodated through passive joints, as illustrated by the red axis in Fig. 3(f). The blue region shown in Fig. 3 has a total mass of 5.4 kg (approximately 78% of the overall exoskeleton mass). From a control perspective, due to the parallel structure, the three relatively heavy actuators are concentrated near the wearer's waist, close to the human center of mass. As a result, regardless of the exoskeleton's posture or the commanded velocity within the workspace, the generated joint velocities remain relatively small. Consequently, the inertia and Coriolis terms in the dynamic model can be kept at relatively low values. During motion following, only the lightweight carbon-fiber links undergo high-speed motion, further reducing dynamic effects and improving comfort and control reliability.

In addition to the human–robot interface described above, this exoskeleton features several design highlights. As shown in Fig. 3(e), the waist ratchet disc allows the bilateral sliding rails to contract toward the center and locks them in place to prevent outward expansion. The adaptive waist–abdominal supports, shown in Fig. 3(g), consist of eight rigid plates that press against the abdomen to counteract large forward or lateral torques generated by the exoskeleton. Together with the sliding rail structure, these plates can self-adjust to fit the wearer's waist and abdominal shape. The upper-arm self-rotation mechanism, shown in Fig. 3(f), adopts a semi-self-locking design: when the exoskeleton applies a compressive force to the elbow, the elbow rotation joint locks; when a tensile force is applied, the joint releases.

To accommodate users with heights ranging from 1.6 m to 1.9 m, the link lengths were carefully optimized, as illustrated in Fig. 1(b) and (c): the radius of the circular

waist guide rail is $R = 100$ mm, $L_{AB} = 282$ mm, $L_{BC} = 200$ mm, $L_{CD} = 120$ mm, $L_{DE} = 250$ mm, $L_{AE} = 128$ mm, and $L_{CF} = 161$ mm.

III. Exoskeleton Control System

To achieve lightweight and modular design of the exoskeleton, meet the requirements of wearing comfort for users, and reduce the development time cost, an exoskeleton control system was designed, including printed circuit board (PCB) design and electrical architecture design. As shown in Fig. 4, the control system mainly consists of a control module, sensing module, actuation module, and power supply module. The RK3588 edge computing board (Rockchip, China) is used as the high-level decision-making core. With its powerful data processing capability, it undertakes complex algorithm execution and system task scheduling, and communicates via UART with the low-level control unit STM32F407VET6 microcontroller. The STM32F407VET6, through its SPI interface, connects to the ADS1256 data acquisition module, which preprocesses multidimensional physical signals collected from two three-dimensional force sensors (Spartan, China) and two MT6835 angle encoders (custom-designed) in the sensing module. These data are used to perceive the human-exoskeleton interaction and perform control. The actuation module consists of four DM4340P joint motors (Damiao, China) and two CyberGear joint motors (Xiaomi, China), all of which are controlled by the microcontroller via a CAN bus. The power supply module consists of a 24V battery and a step-down circuit, providing 24V power for the joint motors in the actuation module and 5V power for all PCBs in the control and sensing modules. All PCBs are independently developed to meet the lightweight design requirements of the exoskeleton.

IV. Kinematics

A. Kinematic Modeling of the Exoskeleton

As shown in Fig. 5(a), the joint coordinate frames of the exoskeleton robot at the zero position (only the left half of the exoskeleton is analyzed) are defined as follows. The world coordinate frame W coincides with the pelvic position of the human body, and coordinate frame O coincides with the circular guide rail. The remaining joint coordinate frames are attached to the corresponding joints of the planar five-bar linkage. All joint coordinate frames are defined as right-handed systems.

For convenience of calculation, the x- and y-axis of the joint coordinate frames at points A, B, C, D, and E are aligned with the y- and z-axis of the world frame, respectively, and the z-axis of the motor joint frames are aligned with the z-axis of the world frame. Let θ_i $(i = 1, 2, 3)$ represent the three active joint rotation angles. The kinematics of the planar five-bar linkage $ABCDE$ can be derived geometrically.

As shown in Fig. 5(b), the mapping relationships φ_1, φ_4, and φ_2, θ_3 are given by:

$$\varphi_1 = \theta_2 + 0.934, \varphi_4 = \theta_3 + 0.145. \tag{1}$$

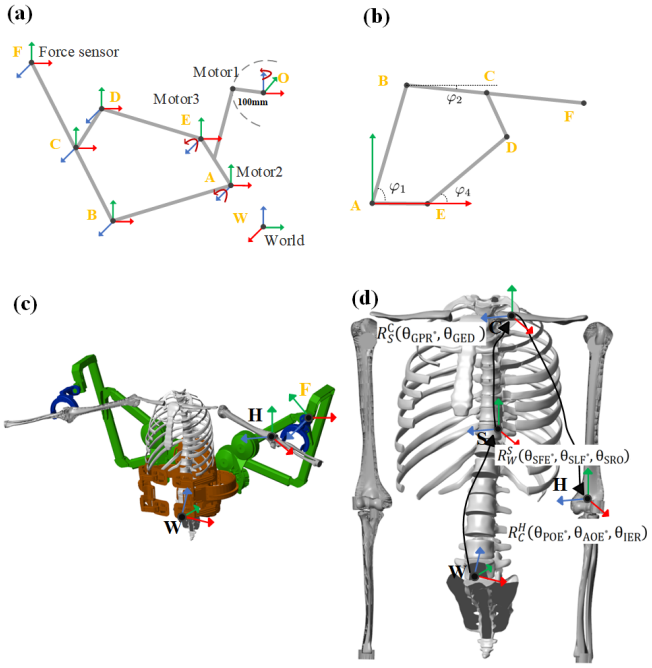

Fig. 5. (a) Joint coordinate frames of the left half of the exoskeleton; (b) Joint coordinate frames of the planar five-bar parallel mechanism; (c) Coupling between the exoskeleton and the human skeleton; (d) Coordinate frames of the human upper-body skeleton (red: x-axis, green: y-axis, blue: z-axis).

The coordinates of point B are:

$$x_b = L_{AB} \cdot \cos(\varphi_1), y_b = L_{AB} \cdot \sin(\varphi_1). \tag{2}$$

The coordinates of point D are:

$$x_d = L_{AE} + L_{DE} \cdot \cos(\varphi_4), y_d = L_{DE} \cdot \sin(\varphi_4). \tag{3}$$

The coordinates of point C are:

$$x_c = x_b + L_{BC} \cdot \cos(\varphi_2), y_c = y_b + L_{BC} \cdot \sin(\varphi_2), \tag{4}$$

where

$$A = 2 \cdot L_{BC} \cdot (x_d - x_b), B = 2 \cdot L_{BC} \cdot (y_d - y_b), \tag{5}$$

$$C = L_{BC}^2 + (x_d - x_b)^2 + (y_d - y_b)^2 - L_{CD}^2, \tag{6}$$

and

$$\varphi_2 = 2 \cdot \text{atan2}\left(\frac{B \pm \sqrt{A^2 + B^2 - C^2}}{A + C}\right). \tag{7}$$

Therefore, the coordinates of point C can be calculated as:

$$x_c = x_b + L_{BC} \cdot \cos(\varphi_2), y_c = y_b + L_{BC} \cdot \sin(\varphi_2). \tag{8}$$

The coordinates of point F are:

$$\begin{aligned} x_f &= x_b + (L_{BC} + L_{CF}) \cdot \cos(\varphi_2), \\ y_f &= y_b + (L_{BC} + L_{CF}) \cdot \sin(\varphi_2). \end{aligned} \tag{9}$$

Based on the established joint coordinate frames and the relative joint relationships, the forward kinematic model parameters can be obtained, as summarized in Table 1.

TABLE I

FORWARD KINEMATIC MODEL PARAMETERS OF THE EXOSKELETON

Link	x **trans. (mm)**	y **trans. (mm)**	z **trans. (mm)**	x **rot. (rad)**	y **rot. (rad)**	z **rot. (rad)**
–	0	0	0	0	0	π
W-O	-105	-390	129	0	0	θ_1
O-A	300	203	270	$\pi/2$	0	0
A-C	x_c	y_c	0	0	0	0
C-F	$L_{CF}\cos\varphi_2$	$L_{CF}\sin\varphi_2$	190	0	0	0

TABLE II

RANGE OF MOTION (ROM) OF HUMAN UPPER-BODY JOINT DOFS

DOF	**MIN (°)**	**MAX (°)**
θ_{SFE}	$-50°$	$50°$
θ_{SLF}	$-40°$	$40°$
θ_{SRO}	$-45°$	$45°$
θ_{GPR}	$-10°$	$30°$
θ_{GED}	$-15°$	$5°$
θ_{POE}	$0°$	$165°$
θ_{AOE}	$-45°$	$85°$
θ_{IER}	$-135°$	$135°$

Therefore, the homogeneous transformation matrix from the world frame W to the three-dimensional force sensor frame F, T_W^F, can be expressed as:

$$T_W^F = T_W^O T_O^A T_A^C T_C^F. \tag{10}$$

Since there are only three active degrees of freedom, the three active joint angles are known, and the position and orientation of the force sensor can be uniquely determined. In Fig. 5(c), the humerus frame H and the exoskeleton force sensor frame F are connected through the three passive joints shown in Fig. 3(f), which enable the pose transformation between the two frames.

All joints are mechanically and software-limited to prevent the mechanism from exceeding its maximum range of motion, while also cleverly avoiding output singularities [18]. In the exoskeleton workspace, input singularities are reasonably distributed. As shown in the figure, when points B, C, and D are collinear, the force along BCD is equivalent to the effective force at the end-effector. At this moment, the Jacobian matrix $\boldsymbol{J}$ becomes singular. Therefore, a joint encoder is introduced at point B, allowing the end-effector position to be calculated even at input singularities, while also reducing errors caused by mechanical backlash.

B. Kinematic Modeling of the Human Upper Body

This exoskeleton covers 8-DOF of the human upper body, which can be divided into three groups: a 3-DOF spine (SP), a 2-DOF sternoclavicular joint (SC), and a 3-DOF glenohumeral joint (GH). The spine possesses highly complex DOFs, where the lumbar and thoracic vertebrae cooperate to enable trunk flexion and lateral bending. For modeling purposes, the spine is simplified to 3-DOF, as shown in Fig. 2(a). The sternoclavicular joint involves multiple independent DOFs of the clavicle and scapula, which makes its motion complicated. However, most of these DOFs are redundant with the rotational DOFs of the glenohumeral joint. Therefore, we select protraction/retraction (GPR) and elevation/depression (GED) as the two representative DOFs, as shown in Fig. 2(b). The glenohumeral joint exhibits small translations relative to the sternoclavicular joint, which are primarily generated by SC joint motion and can be considered negligible. Hence, the glenohumeral joint can be modeled as a ball-and-socket joint, and three DOFs are selected for analysis: Plane of Elevation (POE), Angle of Elevation (AOE), and Internal/External Rotation (IER) [19], [20].

To build a more realistic human upper-body model, we use human modeling in Siemens NX with the ANSUR anthropometric database. The required range of motion (ROM) for activities of daily living (ADL) was derived from the maximum values of the related work and translated to the ISB coordinate system [21], [22], [23]. The human upper-body coordinate frame definitions are shown in Fig. 5(c), where the world frame W is aligned with the human pelvis, frame S is aligned with the spine, and θ_{SFE}, θ_{SLF}, and θ_{SRO} represent the DOF of the spine. Frame C is aligned with the sternoclavicular joint, with θ_{GPR} and θ_{GED} describing the SC motion. Frame H is aligned with the humerus, with θ_{POE}, θ_{AOE}, and θ_{IER} representing the GH joint motion. The ROMs of all DOF are summarized in Table II.

V. EXPERIMENTS

A. Verification of Kinematics

To verify the correctness of the previously derived kinematics, we performed a circular trajectory tracking experiment within the exoskeleton's workspace. The tracking task was implemented by solving the inverse kinematics problem of the left half of the exoskeleton using a gradient descent algorithm, enabling the end-effector to follow a prescribed circular trajectory. In the experiment, a target circular trajectory with a center at $[0.4812, 0.2436, 0.2570]$ m and a radius of 0.05 m was generated based on time parameters. As shown in Fig. 6(a), the tracking error between the actual and target positions was less than 10^{-3} m, which is acceptable under normal operating conditions. This result confirms the correctness of the forward and inverse kinematic analyses. However, around $t = 1$ s, noticeable oscillations were observed in joint motors 2 and 3, resulting in fluctuations of the end-effector position. This phenomenon occurs because the five-bar parallel mechanism entered an *input singularity*, at which the effective force at the end-effector reaches its maximum. To obtain the end-effector position under such conditions, an angular encoder was installed at the passive

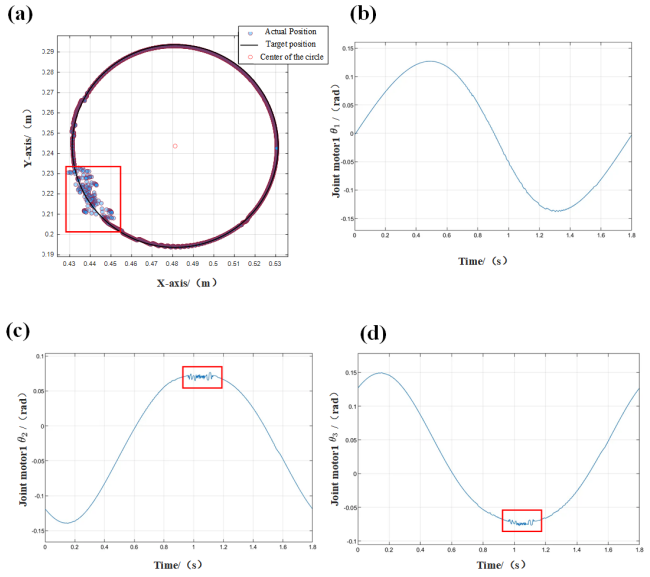

Fig. 6. End-effector tracking performance comparison: (a) X–Y plane circular trajectory tracking; (b) Joint motor 1 position tracking; (c) Joint motor 2 position tracking; (d) Joint motor 3 position tracking.

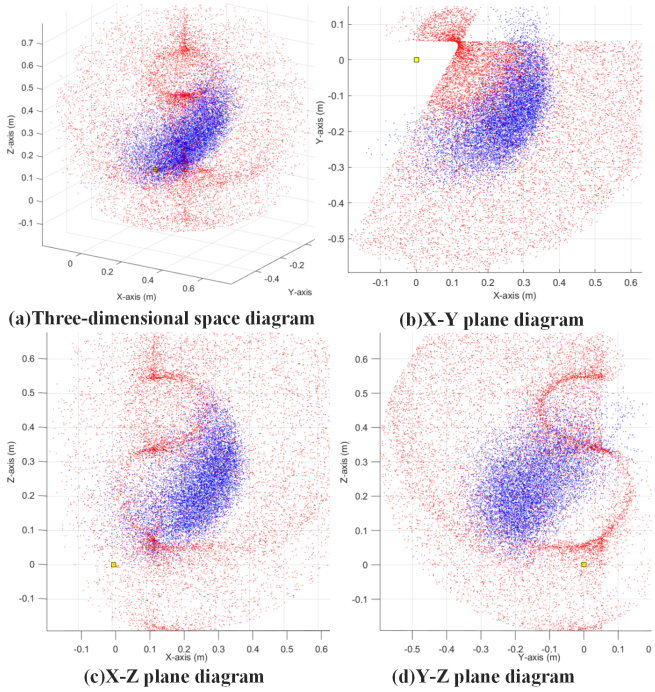

Fig. 7. Workspace comparison between the upper-body exoskeleton and the human elbow (red point cloud represents the exoskeleton workspace, blue point cloud represents the human elbow workspace).

joint (Fig. 3(d)), allowing the computation of the end-effector position even when the exoskeleton operates near input singularities.

B. Workspace Analysis

To evaluate whether the upper-limb exoskeleton design satisfies the workspace of the entire upper body, it is crucial to ensure that there is no collision between the exoskeleton and the human limbs and trunk, and that the exoskeleton end-effector workspace fully matches the human's actual range of motion. In Section 3, a kinematic model of the upper body was established using the human model in Siemens NX with the ANSUR anthropometric database. The upper body skeleton was simplified as a serial robot consisting of eight rotational links, and local coordinate frames were assigned to each joint to map joint space to the end-effector space. A Monte Carlo sampling method [24] with random sampling was used to generate joint configurations, with each joint range defined as in Table II, and 5000 random samples were taken. The sampled points were then plotted in Cartesian space to obtain the point cloud representation of the human elbow workspace. The same procedure was applied to the exoskeleton model to obtain its end-effector point cloud. As shown in Fig. 7, the exoskeleton workspace fully covers and even exceeds the human elbow workspace, which theoretically indicates that the exoskeleton satisfies the workspace requirements of the upper body.

Further experimental validation was performed by having a subject wear the exoskeleton and complete five extreme motions. As illustrated in Fig. 8, analysis of these five motions shows that the parallel exoskeleton can perfectly accommodate the motion space of the human upper body without collision with the trunk. In contrast, a conventional serial exoskeleton may cause collision at the posterior shoulder during Motion 1 (Fig. 8b) when the arm is raised overhead. The proposed parallel design places the actuators behind the waist, providing sufficient clearance for the posterior shoulder and back. During Motion 2 (Fig. 8c), when the arms are abducted laterally, a serial exoskeleton can only follow arm motion but cannot synchronize with the scapulohumeral rhythm, potentially causing shoulder or even head injury. Our design, by covering the sternoclavicular joint DOF, avoids interference with natural motion patterns (such as scapulohumeral rhythm) and reduces the risk of shoulder joint injury. During Motion 3 (Fig. 8d), when the arms are extended backward, the waist actuator position can be adjusted to prevent collision. The parallel design also enables large forward reach, allowing the user to perform Motion 4 (Fig. 8e) forward forearm extension and Motion 5 (Fig. 8f) spinal flexion, showing that the exoskeleton covers the spinal DOF and effectively reduces stiffness and heaviness in the upper body. This feature also accommodates users of different body sizes and arm lengths.

In conclusion, under the same number of active DOF, the proposed parallel exoskeleton offers superior workspace coverage compared with a serial exoskeleton. Moreover, its loosely coupled design provides greater motion flexibility and adaptability, better matching the complex movement patterns of the human body. In practical applications, this design improves wearing comfort and significantly reduces motion constraints caused by excessive structural rigidity.

VI. Conclusion

In this study, a novel loosely coupled parallel upper-body exoskeleton was proposed for overhead task assistance.

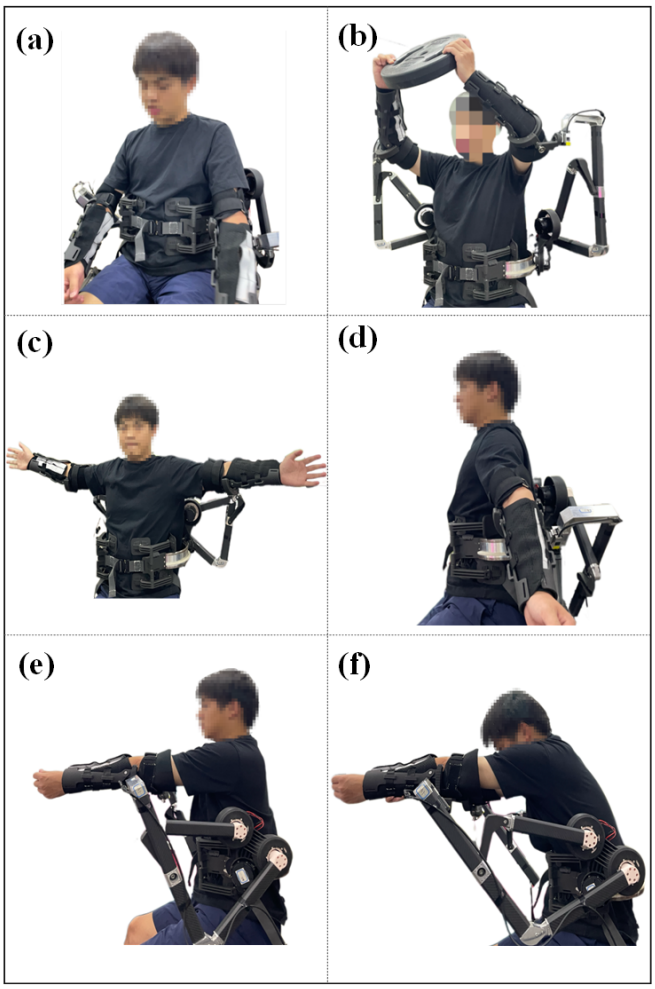

Fig. 8. Different motions performed while wearing the exoskeleton: (a) Initial posture: arms naturally lowered; (b) Motion 1: raising both arms to maximum elevation (commonly used for overhead operations); (c) Motion 2: abducting both arms horizontally to the sides; (d) Motion 3: extending both arms backward to maximum angle; (e) Motion 4: extending arms forward while keeping forearms straight; (f) Motion 5: flexing arms forward.

The structural design characteristics, as well as the custom-designed electrical system architecture and control circuitry, were described in detail. Furthermore, the kinematics and statics of the parallel structure were analyzed and experimentally validated. An experimental prototype platform was built, and workspace analysis was conducted with a subject wearing the exoskeleton. The results demonstrate that the parallel structure allows the exoskeleton to follow human motion more flexibly while providing sufficient workspace coverage. Future work will focus on implementing impedance and admittance control strategies to achieve compliant motion and active assistance.

REFERENCES

[1] C. Latella, "Analysis of human whole-body joint torques during overhead work with a passive exoskeleton," *IEEE Trans. Hum.-Mach. Syst.*, vol. 52, no. 5, pp. 1060–1068, Oct. 2022.

[2] H. Jo, O. B. Lim, Y. S. Ahn, S. J. Chang, and S. B. Koh, "Negative impacts of prolonged standing at work on musculoskeletal symptoms and physical fatigue: The fifth Korean working conditions survey," *Yonsei Med. J.*, vol. 62, pp. 510–519, Jun. 2021.

[3] O. Flor-Unda, B. Casa, M. Fuentes, *et al.*, "Exoskeletons: Contribution to occupational health and safety," *Bioengineering*, vol. 10, no. 9, p. 1039, 2023.

[4] E. P. Lamers, J. C. Soltys, K. L. Scherpereel, *et al.*, "Low-profile elastic exosuit reduces back muscle fatigue," *Sci. Rep.*, vol. 10, p. 15958, 2020.

[5] L. Van Engelhoven, N. Poon, H. Kazerooni, *et al.*, "Evaluation of an adjustable support shoulder exoskeleton on static and dynamic overhead tasks," in *Proc. Human Factors and Ergonomics Soc. Annu. Meeting*, vol. 62, no. 1, pp. 804–808, 2018.

[6] I. Pacifico, A. Scano, E. Guanziroli, *et al.*, "An experimental evaluation of the proto-mate: a novel ergonomic upper-limb exoskeleton to reduce workers' physical strain," *IEEE Robot. Autom. Mag.*, vol. 27, no. 1, pp. 54–65, 2020.

[7] L. Zheng, Q. Wu, Y. Zhu, *et al.*, "Design and evaluation of a reconfigurable 7-DOF upper limb rehabilitation exoskeleton with gravity compensation," in *Proc. IEEE Int. Conf. Robot. Autom. (ICRA)*, 2024, pp. 190–196.

[8] L. Grazi, E. Trigili, G. Proface, *et al.*, "Design and experimental evaluation of a semi-passive upper-limb exoskeleton for workers with motorized tuning of assistance," *IEEE Trans. Neural Syst. Rehabil. Eng.*, vol. 28, no. 10, pp. 2276–2285, 2020.

[9] L. Grazi, E. Trigili, N. Caloi, *et al.*, "Kinematics-based adaptive assistance of a semi-passive upper-limb exoskeleton for workers in static and dynamic tasks," *IEEE Robot. Autom. Lett.*, vol. 7, no. 4, pp. 8675–8682, 2022.

[10] H. Liu, K. Fang, L. Chen, *et al.*, "Implementation of a long-lasting, untethered, lightweight, upper limb exoskeleton," *IEEE/ASME Trans. Mechatronics*, 2024, doi: 10.1109/TMECH.2024.1083-4435.

[11] X. Zhou and L. Zheng, "Model-based comparison of passive and active assistance designs in an occupational upper limb exoskeleton for overhead lifting," *IISE Trans. Occup. Ergon. Hum. Factors*, vol. 9, no. 3-4, pp. 167–185, 2021.

[12] B. M. Otten, R. Weidner, and A. Argubi-Wollesen, "Evaluation of a novel active exoskeleton for tasks at or above head level," *IEEE Robot. Autom. Lett.*, vol. 3, no. 3, pp. 2408–2415, 2018.

[13] S. Ramesh and M. Plecnik, "A direct-drive five-bar manipulator with tuned directional first-order kinematics for low energy consumption in vertical loading," *Int. J. Robot. Res.*, vol. 44, no. 2, pp. 317–338, 2025.

[14] S. Ramesh, P. M. Wensing, and M. Plecnik, "Output mode switching for parallel five-bar manipulators using a projection-based direct collocation method," in *Proc. 6th Int. Conf. Reconfigurable Mech. Robot. (ReMAR)*, 2024, pp. 1–8.

[15] B. Kim and A. D. Deshpande, "An upper-body rehabilitation exoskeleton Harmony with an anatomical shoulder mechanism: Design, modeling, control, and performance evaluation," *Int. J. Robot. Res.*, vol. 36, no. 4, pp. 414–435, 2017.

[16] U. Keller, H. J. van Hedel, V. Klamroth-Marganska, *et al.*, "ChARMin: The first actuated exoskeleton robot for pediatric arm rehabilitation," *IEEE/ASME Trans. Mechatronics*, vol. 21, no. 5, pp. 2201–2213, 2016.

[17] G. Ferreira, J. Gaspar, C. Fujão, *et al.*, "Piloting the use of an upper limb passive exoskeleton in automotive industry: Assessing user acceptance and intention of use," in *Int. Conf. Appl. Human Factors Ergonomics*, Cham: Springer, 2020, pp. 342–349.

[18] P. B. Edwards, A. Baskar, C. Hills, M. Plecnik, and J. D. Hauenstein, "Output mode switching for parallel five-bar manipulators using a graph-based path planner," in *Proc. IEEE Int. Conf. Robot. Autom. (ICRA)*, 2023, pp. 9735–9741.

[19] Y. Zimmermann, M. Sommerhalder, P. Wolf, *et al.*, "ANYexo 2.0: A fully actuated upper-limb exoskeleton for manipulation and joint-oriented training in all stages of rehabilitation," *IEEE Trans. Robot.*, vol. 39, no. 3, pp. 2131–2150, 2023.

[20] Y. Zimmermann, A. Forino, R. Riener, *et al.*, "ANYexo: A versatile and dynamic upper-limb rehabilitation robot," *IEEE Robot. Autom. Lett.*, vol. 4, no. 4, pp. 3649–3656, 2019.

[21] S. Namdari, G. Yagnik, D. D. Ebaugh, *et al.*, "Defining functional shoulder range of motion for activities of daily living," *J. Shoulder Elbow Surg.*, vol. 21, no. 9, pp. 1177–1183, 2012.

[22] G. Wu, F. C. T. Van der Helm, H. E. J. Veeger, *et al.*, "ISB recommendation on definitions of joint coordinate systems of various joints for the reporting of human joint motion—Part II: shoulder, elbow, wrist and hand," *J. Biomech.*, vol. 38, no. 5, pp. 981–992, 2005.

[23] G. Wu, S. Siegler, P. Allard, *et al.*, "ISB recommendation on definitions of joint coordinate system of various joints for the reporting of human joint motion—Part I: ankle, hip, and spine," *J. Biomech.*, vol. 35, no. 4, pp. 543–548, 2002.

[24] Y. Guan and K. Yokoi, "Reachable space generation of a humanoid robot using the Monte Carlo method," in *Proc. IEEE/RSJ Int. Conf. Robot. Syst.*, Beijing, China, 2006, pp. 1984–1989.